Published in final edited form as:

Structure. 2015 March 03; 23(3): 505–516. doi:10.1016/j.str.2014.12.017.

Allosteric effects of the oncogenic RasQ61L mutant on Raf-RBD

Susan K. Fetics[1,2], **Hugo Guterres**[1], **Bradley M. Kearney**[1,2], **Greg Buhrman**[2], **Buyong Ma**[3], **Ruth Nussinov**[3,4], **Carla Mattos**[1,2]

[1]Department of Chemistry and Chemical Biology, Northeastern University, Boston, MA 02115

[2]Department of Molecular and Structural Biochemistry, North Carolina State University, Raleigh, NC 27695

[3]Basic Science Program, Leidos Biomedical Research, Inc., Cancer and Inflammation Program, National Cancer Institute, Frederick, MD 21702

[4]Sackler Inst. of Molecular Medicine Department of Human Genetics, Sackler School of Medicine, Tel Aviv University, Tel Aviv 69978, Israel

Summary

The Ras/Raf/MEK/ERK signal transduction pathway is a major regulator of cell proliferation activated by Ras-GTP. The oncogenic mutant RasQ61L is not able to hydrolyze GTP in the presence of Raf and thus is a constitutive activator of this mitogenic pathway. The Ras/Raf interaction is essential for the activation of the Raf kinase domain through a currently unknown mechanism. We present the crystal structures of the Ras-GppNHp/Raf-RBD and RasQ61L-GppNHp/Raf-RBD complexes that, in combination with MD simulations, reveal differences in allosteric interactions leading from the Ras/Raf interface to the Ras calcium-binding site and to the remote Raf-RBD loop L4. In the presence of Raf the RasQ61L mutant has a rigid switch II relative to the wild type and increased flexibility at the interface with switch I, which propagates across Raf-RBD. We show that in addition to local perturbations on Ras, RasQ61L has substantial long-range effects on the Ras allosteric lobe and on Raf-RBD.

Introduction

Ras proteins are small monomeric GTPases that function as molecular switches in a number of signal transduction networks that control cell proliferation, differentiation and survival (Cox and Der, 2010). Its mutants are found in about 20% of human cancers (Prior et al., 2012). Signal propagation through Ras is dependent on the bound nucleotide. In the GDP-bound form, the active site composed of the P-loop (residues 10-17) and highly disordered switch I (residues 30-40) and switch II (residues 60-76) regions, samples a range of

Contact information: Carla Mattos, c.mattos@neu.edu.

Accession Numbers

Coordinates and structure factors are deposited in the PDB: Ras/Raf-RBD, 4G0N and RasQ61L/Raf-RBD, 4G3X.

conformations that exclude effector binding. When bound to GTP, Ras recruits effector proteins, which in turn are activated for specific protein-protein interactions that ultimately lead to a change in cell behavior (Cox and Der, 2010). This nucleotide cycle is regulated by Guanine nucleotide Exchange Factors (GEFs) and GTPase Activating Proteins (GAPs). The three Ras isoforms, H-Ras, K-Ras and N-Ras, have identical effector binding regions and nucleotide-binding sites located in the N-terminal half of the catalytic domain (effector lobe). They differ at the C-terminus hypervariable region (HVR) and to a much lesser extent in the second half of the catalytic domain (allosteric lobe) distal from the active site (Buhrman et al., 2011b). H-Ras has therefore been used as representative for the structure of all three isoforms at the interface with effector and regulator proteins.

The Ras/Raf/MEK/ERK mitogen activated signaling cascade is involved in the control of cell proliferation and is associated with a variety of aggressive human cancers (Drosten et al., 2010). C-Raf (also known as Raf-1) is a protein of 648 amino acid residues with the N-terminal half containing two highly conserved regions 1 and 2 (CR1 and CR2), and the C-terminal half containing the conserved kinase domain (CR3) (Roskoski, 2010). CR1, CR2 and CR3 are also present in the two other human isoforms A-Raf and B-Raf, although outside of these regions the three isoforms differ substantially (Roskoski, 2010). The CR1 contains two Ras binding domains: the Ras Binding Domain, Raf-RBD (residues 51-131), which binds Ras with an affinity of 18 nM; and the Cysteine Rich Domain, Raf-CRD (residues 139-184), which binds with a much lower affinity of 20 μM (Thapar et al., 2004) (Figure 1). The binding of C-Raf-CRD to Ras is enhanced by farnesylation of Ras and requires the coordination of two zinc ions by CRD residues (Thapar et al., 2004). Both domains are required for Raf activation by Ras and for Raf membrane localization *in vivo* (Bondeva et al., 2002), but the mechanism through which the interaction with Ras leads to the activation of the kinase domain is currently not known.

In spite of the importance of the Ras/Raf complex, the best model to date is that of a complex between Raf-RBD and a Ras homologous protein, Rap1A, in which switch I residues 30 and 31 have been mutated to those found in Ras (dubbed Raps) (PDB code 1GUA), resulting in identical switch I sequences between Ras and the mutant Raps (Nassar et al., 1996). Although the Raps/Raf-RBD complex has served as a good overall model of the interaction, recent work from our laboratory (Buhrman et al., 2010; Buhrman et al., 2011a) and others (Spoerner et al., 2010) has shown that Raf has an important influence on the structure of Ras and conformational states associated with hydrolysis of GTP to GDP. These conformational states involve switch I, which is well modeled in Raps, but they also involve switch II, which has seven residues that are different between Ras and Rap, and therefore is most likely affected differently by Raf-RBD.

We have shown that in crystals with symmetry of the R32 space group, switch II is free of crystal contacts and is allosterically coupled to a site on the allosteric lobe at the interface between helix 3/loop 7/helix 4. Upon binding calcium and acetate at that site there is a clear disorder to order transition that places catalytic residue Q61 in the active site, interacting directly with a water molecule that bridges between switch I residue Y32 and the γ-phosphate of GTP (the bridging water molecule) in a conformation that we propose is poised for intrinsic hydrolysis (Buhrman et al., 2010). Interestingly, this crystal form has switch I

stabilized precisely in the conformation observed in the Raps/Raf-RBD complex, including the bridging water molecule. Based on this observation and the fact that it has been shown by NMR that the binding of Raf promotes a conformation competent for intrinsic hydrolysis (Spoerner et al., 2010), we hypothesized that Raf plays an important role in the allosteric activation of intrinsic hydrolysis by stabilizing switch I, such that switch II can complete the active site modulated by the allosteric switch (Buhrman et al., 2010). This hypothesis was supported by the oncogenic mutant RasQ61L which crystallized with symmetry of the same space group R32. Unlike the wild type which has a disordered switch II in the absence of bound calcium and acetate, switch II in this mutant is ordered to a conformation that interferes with hydrolysis of GTP and that we now call the anticatalytic conformation (Buhrman et al., 2010; Buhrman et al., 2007; Holzapfel et al., 2012; Johnson and Mattos, 2013). In this conformation the bridging water molecule is absent and Y32 makes a direct H-bond with the γ-phosphate of GTP, while switch II closes over the active site, isolating it from bulk solvent (Buhrman et al., 2007). We showed that the RasQ61L mutant was able to hydrolyze GTP in the absence of Raf, albeit slower than wild type, but that in the presence of Raf there was no observed hydrolysis (Buhrman et al., 2011a; Buhrman et al., 2007). Furthermore, signaling through the Ras/Raf/MEK/ERK pathway, but not the Ras/PI3K/Akt pathway, leads to saturating levels of MEK and ERK phosphorylation in the presence of the RasQ61L mutant, suggesting that a long-lived RasQ61L/Raf complex plays a role in increased Ras dependent pERK signaling and is likely to contribute significantly to oncogenesis in RasQ61L mutants (Buhrman et al., 2011a). Interestingly we were able to stabilize the anticatalytic conformation in wild type Ras in the presence of the reducing agent DTE (or DTT), which binds to a site between switch II and helix 3, promoting the conformation we originally observed for RasQ61L (Holzapfel et al., 2012). Our working model, based on structures of Ras in a crystal form where switch I mimics that in the Raps/Raf complex, is that Raf helps to promote the catalytic conformation for intrinsic hydrolysis of GTP on wild type Ras, but that it stabilizes the anticatalytic conformation of the RasQ61L mutant specifically enhancing its oncogenic potential associated with the Ras/Raf/MEK/ERK pathway (Johnson and Mattos, 2013). Because switch II is very different in Raps we have had to base our hypothesis on its behavior in the R32 crystals of Ras alone, assuming that these crystals provide a good approximation of the effect of Raf-RBD on Ras and its mutants. Here we present the X-ray crystal structures of the wild type Ras-GppNHp/Raf-RBD and RasQ61L-GppNHp/Raf-RBD complexes, solved at 2.45 Å and 3.3 Å resolution respectively. The structures confirm that the R32 crystal form indeed provides a good first approximation of both complexes at their molecular interfaces. In addition these structures show that the Q61L mutation affects the allosteric calcium-binding site on Ras and that it has substantial global impacts on the structure of the complex with Raf-RBD. We see clear differences in a Raf-RBD loop (L4) distant from the interface due to the mutation and show, with a series of molecular dynamics simulations and dynamic network analysis, that the Q61L mutation increases the conformational dynamics of the switch II region in Ras in the absence of Raf, quenches the switch II motion in the Ras/Raf-RBD complex, disrupts the connectivity associated with allosteric modulation of the active site in the complex and affects the dynamics of the distant L4 loop in Raf-RBD.

Results

The catalytic domain of Ras and the two Ras-binding domains of Raf (RBD residues 52-131 and CRD residues 139-184) were in the complex set up for crystallization trials both for the wild type and Q61L mutant Ras loaded with the GTP analogue GppNHp: Ras residues 1-166 and Raf residues 52-184. Both wild type and mutant complexes crystallized with symmetry of the space group P321 with one complex per asymmetric unit and structures were solved to 2.45 Å and 3.3 Å resolution respectively. The CRD domain is disordered in both complexes. Thus, while our original intention was to solve the structure of Ras in complex with both Ras binding domains of Raf, what we have is an experimental view of the wild type Ras/Raf-RBD complex and how it is modified by the Q61L mutation. Data collection and structure refinement statistics are given in Table 1.

Wild type Ras bound to Raf-RBD

While the original view of Ras portrayed two Ras states associated with GTP and GDP bound forms, a large body of structural biology work has made it increasingly apparent that Ras-GTP (as seen in structures of Ras-GppNHp) samples distinct conformational substates that have significant implications for signaling: switch I states 1 and 2 observed by NMR (Spoerner et al., 2010), and ordering of switch II in the active site associated with R state and T states observed by X-ray crystallography (Johnson and Mattos, 2013; Kearney et al., 2014). In particular, the R state is characterized by ligand bound in the allosteric site (calcium and acetate in our crystals) and by a highly ordered active site stabilized by water-mediated H-bonding interactions that link the effector and allosteric lobes of Ras through switch I/loop 8/helix 5 and through switch II/helix 3/loop 7 (Kearney et al., 2014). This highly ordered R state is exemplified in the structure with PDB code 3K8Y. The switch I has the same conformation as seen in the Raps/Raf-RBD complex and switch II has a conformation stabilized by R68 through direct and water-mediated interactions that propagate to the N-terminal end of the switch where catalytic residue Q61 is found (Buhrman et al., 2010). As expected, the Ras-GppNHp/Raf-RBD structure shows Raf-RBD interacting at switch I as seen in the Raps/Raf-RBD complex, including the bridging water molecule that we also see in our structure of Ras in the R state (PDB code 3K8Y) (Buhrman et al., 2010). Remarkably, in the crystal form from which we obtained the Ras/Raf-RBD structure the elements of the allosteric switch (switch II, helix 3 and loop 7) are away from crystal contacts as was the case for Ras-GppNHp crystals with symmetry R32 (Buhrman et al., 2010; Buhrman et al., 2007). Furthermore, as with our Ras-GppNHp structure, the Ras-GppNHp/Raf-RBD complex also crystallized under conditions containing 200 mM $Ca(OAc)_2$. The resulting structure of the complex has calcium and acetate bound in the allosteric site, promoting the R state conformation of helix 3/loop 7 and the corresponding structure for switch II that places R68 in position to order the active site residues. However, in this complex there is a molecule of DTE bound between helix 3 and switch II in van der Waals contact with Y96, causing a shift in the position of R68 and a reorientation of its side chain to optimize the interaction with the DTE molecule. This perturbs the water-mediated network that stabilizes switch II and residues 64 and 65 are disordered in this structure (Figure 2A). Q61 adopts a similar conformation as seen in the R state, but due to the change in the H-bonding network that helps order its side chain the side chain amide functional

group is disordered as determined by lack of electron density for these atoms (Figure 2B). Switch II in the R state is normally connected to the main core of the catalytic domain through a series of water molecules that link it to helix 3 residues, stabilizing the entire switch. In our structure of the Ras/Raf-RBD complex the binding of DTE results in the almost complete lack of crystallographic water molecules between switch II and helix 3. Of the network associated with the R state, only two water molecules are present: Wat 312 bridges the backbone carbonyl group of A59 to the backbone amide of G10 in the P-loop and Wat 361 bridges the backbone amide of A59 to the backbone carbonyl of L36 in switch I. In addition, a new water molecule not normally seen in the R state, Wat 313 in the complex, H-bonds simultaneously to the Nε atom of R68 in its new position and the side chain hydroxyl group of Y71. The only other water molecule observed to interact with any of the switch II residues is the nucleophilic water molecule, which as usual H-bonds to the backbone amide of Q61. Interestingly, with the shifted position of R68 and the absence of water molecules between helix 3 and switch II, Y96 relaxes to its position associated with the T state, adding to a T state-like feature of a partially disordered switch II. Thus we have a hybrid structure, where helix 3/loop 7 is in a position to allow ordering of switch II to the R state, but where the binding of DTE disrupts R68 so that some features of the T state begin to appear toward the N-terminal end of switch II.

The RBD domain consists of the classical ubiquitin fold, with 5 β-strands and two α helices connected by loops (β1L1β2L2α1L3β3L4β4L5α2L6β5) (Emerson et al., 1995). In its complex with Ras, the backbone H-bonds between β2 of Ras and β2 of Raf-RBD form an extended intermolecular β sheet (Nassar et al., 1996). In the Ras/Raf-RBD complex presented here the electron density for Raf-RBD has no main chain breaks for residues 54 – 131 and there is electron density for most side chain residues, with notable exceptions being the side chains of residues in the loop 4 (L4) between β-strands 3 and 4 (E104, H105, K106 and K108). The L4 region is in clear contrast to the rest of the Raf-RBD, which is well ordered in the complex.

In addition to the β-sheet interactions that form the interface in the Ras/Raf-RBD complex there are significant interactions between Raf-RBD α1 residues K84, V88 and R89 with switch I residues in Ras as previously determined by NMR, alanine scanning mutagenesis and free energy component analysis (Gohlke et al., 2003; Terada et al., 1999; Thapar et al., 2004). Key interactions based on our structure of the complex are shown in Figure 3 (a comparison with the Raps/Raf-RBD complex is shown in Supplemental Information Figure S1). K84 in α1 interacts simultaneously with Ras residues E31 and D33, and the latter is in a different conformation than seen in the structure of Ras alone. Water molecules 206 and 301 connect Raf-RBD K84 to the α-phosphate of GppNHp on Ras. Raf-RBD residue V88 at the C-terminal end of α1 makes good van der Waals interactions with Ras residues I21 and Y40, which come together from either end of switch I. These three residues form a nice hydrophobic cluster at the interface between the two proteins. The conformation of Ras residue Q25 in the uncomplexed Ras structures overlaps with the position of Raf V88 in the complex and is seen rotated to a different conformer, where it makes a good H-bonding interaction with the side chain of H27, itself in a new conformation in the complex. Raf residue R89 interacts with three Ras residues: it makes a salt bridge with D38, H-bonds to the backbone carbonyl oxygen atom of S39 and stacks over Y40. The side chain of Ras

residue D38 has a different χ_2 dihedral angle relative to that seen in the Ras-GppNHp structure, optimizing the salt bridge to Raf-RBD residue R89.

RasQ61L-GppNHp bound to Raf-RBD

The structure of RasQ61L in the RasQ61L/Raf-RBD complex has helix 3/loop 7 in the R state, with a fully ordered switch II in a conformation that superimposes well on the conformation that we obtained for the RasQ61L-GppNHp structure from crystals with symmetry R32 in the presence of calcium acetate (PDB code 3OIU) (Buhrman et al., 2011a). In that structure there is clear electron density for calcium and acetate in the allosteric site as observed for the wild type. R68 is in its position to facilitate the water-mediated H-bonding interactions that lead to the active site and almost all of the associated water molecules are present between helix 3 and switch II. The active site is perturbed, however, by the fact that in the presence of L61 there is no room for the bridging water molecule and there is a direct H-bonding interaction between Y32 in switch I and the γ-phosphate of GppNHp. This direct H-bond is a feature of the T state and is accompanied by the shift in Y96 also associated with the T state. Perturbation of the water network that results from this shift is seen in this structure as previously described (Buhrman et al., 2011a). In the RasQ61L/Raf-RBD complex there is continuous electron density for the entire switch II and the conformation of its N-terminus as well as the rest of the active site superimpose well on the structure of RasQ61L alone (Figure 4A). The L61 in the active site precludes binding of the bridging water molecule, resulting in a direct H-bond (3.3 Å in the complex) between Y32 and the γ-phosphate of GppNHp (Figure 4B). The structure of RasQ61L/Raf-RBD is solved at 3.3 Å and at this low resolution there are only very few resolved crystallographic water molecules. The nucleophilic water molecule, which is present in virtually all high-resolution structures of Ras is not observed and the cleft between helix 3 and switch II is also devoid of crystallographic water molecules. Consistently, there is no calcium or acetate seen in the allosteric site, although the R state implies its effect on the structure.

In spite of the lower resolution of this structure, continuous electron density is seen for most of the Ras and Raf-RBD molecules, including side chains. There are notable exceptions, however, that given the rest of the structure, are of significance. There is no electron density for the side chain of K84. D33, with which it interacts in the wild type complex, is in the position seen in our structure of the uncomplexed wild type Ras (PDB code 3K8Y). In the wild type complex the position of K84 would clash with the D33 rotamer observed here and in the Ras structure with PDB code 3K8Y (Figure 5A). The fact that there is clear electron density for D33 even at low resolution and that its position overlaps with that seen in the uncomplexed wild type Ras suggests that the RasQ61L mutant has a weaker interaction between Ras switch I D33 and Raf-RBD K84.

With a weakened K84 interaction at switch I, there is a small shift in the N-terminal portion of Raf-RBD helix α1 residues 77-84 in the mutant relative to the wild type complex. These residues directly contact the β-sheet that connect the binding interface to Raf-RBD loop L4 containing residues 103-108 in Raf-RBD. Surprisingly, in the RasQ61L structure there is clear side chain electron density for residues E104, H105 and K108 in Raf-RBD L4. These

side chains are disordered in the wild type complex. Conversely, K109, which is ordered in the wild type complex where it interacts with Q127 and D129, is disordered in the complex with RasQ61L, as indicated by the absence of electron density for this side chain. Consistently, in the mutant complex Q127 is flipped away from K109, making a good H-bond to the backbone carbonyl group of F61, and the side chain of D129 is disordered (Figure 5B). The side chain of L101 at the beginning of L4 is also disordered in the mutant complex.

The interactions involving Q127 connect back to residue R89 at the Ras interface. R89, on Raf-RBD α1, interacts differently in the mutant complex with D38 at the beginning of Ras β2 leading from switch I, possibly influencing a second pathway of communication between switch I and Raf-RBD loop L4 (residues 103-108). This pathway includes R89, R67, F61 and Q127 and was previously determined based on free energy calculations in the modeled complex between Ras and Raf-RBD, looking at pairwise interactions and pathways of energetic coupling (Gohlke et al., 2003). The same group also determined that in the wild type Ras/Raf-RBD complex there is very high flexibility in the Raf-RBD L4 loop (Gohlke et al., 2004). In our structure of the RasQ61L/Raf-RBD, Ras residue S39 and Raf-RBD residues R89, R67 and Q127 have different conformations than seen in our structure of the wild type Ras/Raf-RBD complex (Figure 5B). These residues lead to interactions with K109 as described above and with L101, two residues at either end of L4 with disordered side chains in the mutant complex. There are clear differences in the ways in which wild type Ras and RasQ61L interact with Raf-RBD that propagate to L4, affecting the loop's flexibility in the complex. In particular, the Q61L mutation in Ras has an impact on the way residues K84 and R89 interact at the molecular interface and these local changes affect the connectivity to Raf-RBD L4 residues at the opposite end of the molecule, resulting in diminished flexibility of the loop.

Molecular dynamics simulations show altered flexibility and connectivity due to the Q61L mutation

To understand the effects of the Q61L mutation in uncomplexed Ras and in the Raf-RBD-bound state, we carried out Molecular Dynamics (MD) simulations in explicit solvent for each of the molecules alone and in complex (details in Experimental Procedures). Figures 6A, 6B and 6C show pairwise comparisons of the α-carbon root mean square fluctuations (RMSFs) for Ras residues, highlighting the effects of Raf-RBD binding or of the mutation on the Ras catalytic domain. Figure 6D shows the effects that the wild type and mutant Ras have on the structure of Raf-RBD. A comparison of the RMSFs for wild type Ras alone and in complex with Raf-RBD reveals that there is a significant decrease in switch I flexibility in the complex (Figure 6A). This difference in flexibility is particularly large for residues 30 – 34, the direct site of binding Raf-RBD. In contrast, switch II becomes significantly more flexible upon binding to Raf-RBD. Residues 60 – 67 in particular become highly dynamic, with the RMSF for residue 63 going from 2.5 Å in the uncomplexed protein to nearly 9 Å in the complex with Raf-RBD. There is a slight increase in flexibility at the C-terminus of helix 3 and in loop 7, consistent with this region being adjacent to the more flexible switch II. Most intriguingly, the allosteric site residues R97 and Y137 in helices 3 and 4 that coordinate Ca^{2+} become somewhat more rigid in the complex. The calcium-binding site has

been shown by NMR to be highly mobile and have no specificity for calcium over magnesium in solution (O'Connor and Kovrigin, 2012), whereas magnesium does not bind Ras in our crystals with R32 symmetry (Buhrman et al., 2010). It appears that Ras-RBD binding (mimicked in our crystals) helps order the ion binding pocket and this could increase the calcium specificity in the allosteric site, poising Ras for intrinsic hydrolysis upon calcium signaling as we previously proposed (Buhrman et al., 2010). The increased flexibility of wild type Ras switch II in the complex with Raf-RBD has been reported previously, as has rigidifying effects on the allosteric lobe of wild type Ras due to effector binding (Baussand and Kleinjung, 2013; Gohlke et al., 2004), although the calcium-binding site was not mentioned in these studies.

The effects of the Q61L mutation on the structure of Ras and its complex with Raf-RBD reveal new and important insights. When comparing the RMSFs from the wild type Ras simulations with those of RasQ61L it appears that the mutation has a modest effect on the dynamics of the uncomplexed Ras protein (Figure 6B). The switch I residues have nearly identical RMSFs in both wild type and RasQ61L simulations. Switch II is more flexible in the RasQ61L mutant than in the wild type Ras, with residue 63 having an RMSF of 2.5 Å in the wild type and 5 Å in the mutant, but the effect of the mutation is less than observed for the wild type upon binding Raf-RBD. In contrast to the effect of Raf-RBD binding, the Q61L mutation increases the flexibility of residues R97 and Y137 in the allosteric site. This would make it more difficult for calcium to bind and activate hydrolysis, contributing to a long-lived Ras/Raf complex and constitutive activation of the Ras/Raf/MEK/ERK pathway. The binding of Raf-RBD to RasQ61L results in much larger and global effects due to the mutation (Figure 6C). As is the case for the wild type complex, switch I becomes more rigid in the mutant complex and to a similar extent as in the wild type protein due to direct binding of Raf-RBD in this region. Switch II, on the other hand becomes significantly less flexible upon complex formation and this is associated with a conformation change involving residues 61-65 at the beginning of the switch, towards the conformation seen in the T state structure with PDB code 2RGD (Buhrman et al., 2007). This region forms an ordered 3_{10} helix in the mutant complex, with a hydrogen bond between the main chain carbonyl of E62 and the amide of S65, which is absent in wild type Ras/Raf-RBD. Although not identical to the switch II structure seen in the anticatalytic conformation, this may represent a structure where switch II has moved toward the T state within the context of a helix 3/loop 7 conformation representative of the R state. In contrast to the rigidifying of switch II, the entire β–sheet core of the RasQ61L mutant, as well as additional areas in helix 3 become more flexible upon complex formation relative to RasQ61L alone. Most surprisingly, the P-loop and the N-terminal end of helix 1 becomes significantly more dynamic, with an RMSF of about 2 Å compared to that of 0.5 Å in the uncomplexed RasQ61L. It is clear that the effects of the Q61L mutation, far from being local, substantially alter the dynamics of the mutant, particularly in the context of the complex with Raf-RBD.

The simulation containing Raf-RBD alone, starting from the average NMR structure (Emerson et al., 1995), shows a highly flexible molecule with residue RMSFs much higher than in the complex with either wild type Ras or RasQ61L (Figure 6D). The overall average RMSF for Raf-RBD alone is 2.6 Å, whereas in complex with wild type Ras and RasQ61L they are 1.5 Å and 1.6 Å respectively. Complex formation rigidifies all regions of Raf-RBD,

with large reductions in flexibility seen at the β2 strand, loop L2, α1 and L4. The differences seen in the Raf-RBD residues RMSFs when comparing the complexes with wild type and mutant Ras are consistent with the relative ordering of the residues as described above for the crystal structures, based on the electron density maps. The side chain of Raf-RBD residue K84, which is clearly seen in the crystal structure of the wild type complex but not in the mutant, has increased RMSF in the mutant complex, as do residues 77-86 in α1 that we observed to be slightly shifted in the mutant. This is consistent with a more dynamic interaction at switch I, which in turn could explain the higher RMSF for the P-loop in the RasQ61L/Raf-RBD complex. Loop L4 residues 103 – 108 belong to an area of the Raf-RBD structure for which we observed a higher degree of order based on electron density in the complex with RasQ61L relative to wild type Ras. Consistently the RMSF for this region in the structure is lower in the mutant complex (Figure 6D). This trend is reversed at residues L101 and K109 at either end of L4, which are disordered in the mutant complex but well ordered in the wild type. R89, R67, Q127 and D129, in β-strands 2, 5 and 3 in the pathway that links the interface with Ras to loop L4 also have higher RMSFs in the RasQ61L/Raf-RBD complex relative to the complex with wild type Ras. F61 in β1 is slightly more rigid in the mutant complex, perhaps due to its backbone interaction with the side chain of Q127 (Figure 5B). It is clear both from our crystal structures and from the MD simulations presented here that the previously identified pathway of communication between Ras and L4 in Raf is affected significantly by the Q61L mutation in Ras. Residues in this pathway are consistently more flexible in Raf-RBD when bound to RasQ61L, where the wild type interactions of Q127 and D129 with K109 are not present and loop L4 can achieve a more stable conformation.

In order to gain further insight into possible factors that result in a more rigid L4 in the complex with RasQ61L relative to the wild type complex, we analyzed the conformations of this loop throughout the 90 ns simulations for the two complexes. Although in crystals from which both structures were solved L4 residues 104 – 109 are away from crystal contacts, R100, located before the beginning of L4, is in contact with Raf-RBD residues S120 and I122 of a symmetry-related molecule and this is expected to restrict motion associated with L4 in crystals of both the wild type and mutant complexes. This constraint is not present in the simulations, allowing access to a greater range of conformational states. Even so, Raf-RBD L4 in the wild type complex fluctuates around the position seen in the crystals, resulting in an average MD simulation structure with L4 in a position close to the starting structure. In the complex with RasQ61L, however, E104 flips to make a salt bridge to R100 (Figure 7). This salt bridge is present 69.2% of the 90 ns simulation time and is a key feature of the average MD simulation structure. R100 also forms a salt bridge with E124 and through this interaction it is linked to a series of H-bonds leading to Ras switch I residue E37 at the binding interface. While the connection to L4 is only seen in the mutant complex (it is not observed at all during the simulation of the wild type complex) the pathway connecting the Ras interface to R100 is found in both structures (Figure 7). It propagates from E37 on Ras through a salt bridge to R59 on β1 of Raf-RBD, whose backbone amide H-bonds to the backbone carbonyl group of E124 on β5. This interaction network through the central β-sheet connects two salt bridges at either end of this pathway, which terminates with R100 in an accessible position for docking of the L4 residue E104. In summary, differences

in the RasQ61L interface with Raf-RBD lead to disordered L101 and K109 in the mutant and this appears to be correlated with flipping of L4 so that E104 can interact with R100. This salt bridge is a key feature contributing to the rigidity of L4 in the mutant.

The differences in connectivity between residues in the wild type and mutant complexes can be visualized using dynamic network analysis of the MD simulation trajectories (Sethi et al., 2009). In this analysis, each residue is assigned a node centered on its Cα atom and edges are used to connect nodes with associated residues that interact at least 75% of the time (within 4.5 Å) throughout the 90 ns simulation time. Within the global dynamical network in our complexes there are sub-networks, called community networks, made of nodes that are tightly interconnected within a group and more loosely connected to other groups (Figure 8). There are 10 community networks in the wild type complex (Figure 8A), with the allosteric and active sites residing at opposite extremes of a single community network that connects them, and an interface that leads to Raf-RBD L4 through two distinct communities, divided at Raf-RBD F61, leading to K109. In general, residues at the interface between communities are likely to be key in allosteric communication between distant regions (Sethi et al., 2009) and thus, F61 may be an important residue in this respect. There are only 9 community networks in the mutant. In contrast to the wild type, the allosteric and active sites are in two separate community networks, while the connection from the complex interface to the Raf-RBD L4 is through a single community network that includes the path from E37 at the Ras complex interface to R100 near L4 (Figure 8B).

An analysis of the pathways of communication between the Ras allosteric site and Raf-RBD L4 can be used to assess the strength of allosteric communication between two sites in the complexes (Sethi et al., 2009). The shortest path (optimal path) between R97 in the Ras allosteric site and K109 at the end of Raf-RBD loop L4 was calculated and serves as the main path between the source node (R97) and the sink node (K109) (Figure 9). The alternate paths (suboptimal paths) were also determined for both complexes. There are 39 and 6 suboptimal paths in the wild type and mutant complexes respectively, indicative of a high connectivity between the two sites in the wild type that is not present in the mutant. The optimal path in the wild type protein involves helix 3 and switch II on Ras, as well F61, while suboptimal paths also include the Ras β-sheet core. Note that the optimal and several suboptimal paths are directed through F61 in the wild type complex, again consistent with the idea that this residue is key in the allosteric communication between the Ras allosteric site and Raf-RBD loop L4. Interestingly, the only path leading from the Ras allosteric site to the Ras/Raf interface in the mutant complex goes through the core β-sheet and does not include switch II.

Discussion

Over the past several years we have accumulated structural evidence suggesting that binding of Raf-RBD would be expected to order the switch II of RasQ61L to an anticatalytic conformation that would keep Ras in its GTP-bound state (Buhrman et al., 2010; Buhrman et al., 2011a; Buhrman et al., 2007; Holzapfel et al., 2012). Our insight is based on structures of uncomplexed Ras and its mutants solved from a crystal form in which switch I is in the same conformation as seen in the Raps/Raf-RBD complex, the only experimental model

available for nearly 20 years to represent the Ras/Raf-RBD interaction (Nassar et al., 1996). The Ras/Raf-RBD complexes presented here not only support our insights based on the structures of Ras crystallized with R32 symmetry, but also provide information on how the Ras mutation changes the local dynamics at the RasQ61L/Raf-RBD interface, which propagate across the Ras and Raf-RBD structures to areas likely to directly impact activity.

Our analysis of the crystal structures of the wild type and mutant complexes, coupled with results of MD simulations, clearly links the Q61L mutation to residues L101 and K109, at either end of Raf-RBD loop L4. The connection is through a pathway of communication that had been previously identified for the wild type Ras/Raf-RBD complex from simulations based on a homology model starting with the Raps/Raf-RBD structure (Gohlke et al., 2003; Gohlke et al., 2004). The MD simulations presented here show that while the L61 residue has the effect of significantly increasing the flexibility of switch II, it has the opposite effect in the complex with Raf-RBD, where switch II becomes more rigid. This is in spite of the fact that binding of Raf-RBD to the wild type protein dramatically increases the flexibility of switch II. Stabilization of switch I in the mutant complex positions Y32 such that it can participate in a hydrophobic cluster involving switch II residues, with L61 at its core (Buhrman et al., 2011a; Buhrman et al., 2007). In contrast to switch I and switch II, the P-loop becomes more flexible relative to the wild type protein (uncomplexed or in complex with Raf-RBD) or to uncomplexed RasQ61L. These changes particularly affect the interactions of Raf-RBD residues R67 and K84 at the interface with Ras, both of which have higher RMSFs in the mutant complex, with repercussions throughout the Raf-RBD structure ultimately resulting in disordered L101 and K109 in RasQ61L/Raf-RBD (Figure 5). The fact that K109 in the mutant complex has more flexible interactions with Q127 and D129 than in the wild type, coupled to increased L101 flexibility, may allow a predominant conformation of L4 where residue E104 forms a salt bridge with R100, not seen in the complex with wild type Ras (Figure 7). The long-range effect of the Q61L mutation is also clearly seen in our community network analysis, where the mutation results in a disconnection between residues in the allosteric and active sites, and where the connection between the interface and Raf-RBD L4 becomes directed through a single community network, which includes the R100 residue that interacts with E104. In the wild type complex, the presence of several suboptimal paths indicates degeneracy of communication, with good connection between the Ras allosteric site and Raf-RBD loop L4. In contrast, in the mutant complex there is only a single path leading from the Ras allosteric site to the interface with Raf-RBD, which goes from helix 3 through the β-sheet core and does not include switch II. Of note, R100 is primarily engaged in a salt bridge with E104 and participates in the link to K109 only through one of the suboptimal paths. The number of suboptimal paths leading from the complex interface to L4 is greatly reduced in the mutant relative to the wild type complex. Overall, communication between the allosteric site in Ras and L4 in Raf-RBD is weak in the mutant complex, indicative of a severed allosteric network between the two sites. The discovery that the Q61L mutation has a global effect is highly significant and novel, as the current assumption is that the effects of oncogenic mutations are local, with the common active site mutants at G12, G13 and Q61 affecting intrinsic hydrolysis rates and sensitivities to GAPs, thus prolonging the duration of the GTP-bound form of Ras.

It has become increasingly apparent that Ras oncogenic mutants occur at very different rates in different cancers and that they affect distinct pathways in the cell (Prior et al., 2012). The G12V and Q61L mutants, for instance, behave differently in terms of their interactions with GAPs (Gremer et al., 2008) and we have shown that they have different switch II structures and respond differently to allosteric modulation associated with intrinsic hydrolysis (Buhrman et al., 2011a; Buhrman et al., 2007). Of particular note, they respond differently to Raf both in terms of their hydrolysis rates and in terms of MEK and ERK phosphorylation (Buhrman et al., 2011a). RasQ61L cannot hydrolyze GTP in the presence of Raf-RBD and it aggressively activates the Ras/Raf/MEK/ERK pathway (Buhrman et al., 2011a; Buhrman et al., 2007). This correlates well with the prevalence of the Ras Q61 mutations in melanomas, which can also be driven by V600 mutations in Raf (Dhomen and Marais, 2007). Given the unique relationship between Ras mutated at residue 61 and Raf at the structural, biochemical and cell biology levels, it is imperative that we make progress in understanding the mechanisms through which the Q61 mutants constitutively activate Raf kinase. Yet, to date, there is no definitive information on the molecular mechanism through which activation of the Raf kinase domain is effected by the Ras-GTP/Raf interaction, even in the case of the wild type protein. We focused here on progressing beyond the current understanding of local effects due to the Q61L mutation and showed that it has a global impact on structure, particularly in the complex with Raf-RBD. In addition to stabilizing switch II, L61 promotes greater flexibility in the Ras allosteric calcium-binding site and in the pathway of communication linking the Ras/Raf-RBD interface to the Raf-RBD loop L4, which in turn has been proposed as a key element in activating the kinase domain (Gohlke et al., 2003). Elucidating the ways in which structural pathways of communication in protein complexes within signaling networks are affected by oncogenic mutants is key in promoting novel approaches to target Ras in human cancers (Nussinov et al., 2013). The present work represents a shift in paradigm in the way we regard the effects of oncogenic Ras mutations and opens new exciting venues for future research in this area.

Experimental Procedures

Protein purification, crystallization and structure determination

Wild type H-Ras and H-RasQ61L were expressed as truncated versions, residues 1-166 as previously published (Buhrman et al., 2011a; Buhrman et al., 2007). Purification and loading of GppNHp have also been published (Buhrman et al., 2007). A C-Raf construct (GB1_Raf-RBD-CRD) containing an N-terminal B1 immunoglobulin-binding domain of streptococcal protein G (GB1 domain) (for increased protein solubility and expression levels) (Huth et al., 1997) followed by a thrombin cleavage site and the two Ras binding domains consisting of residues 52-184 was cloned by Genewiz (South Plainfield, NJ, USA) into the EcoRI and BamHI restriction sites on the Champion pET302/NT-His vector (Invitrogen). The protocol for the expression and purification of this protein in complex to either wild type Ras or RasQ61L is found in the Supplemental Information. The purified complexes were concentrated to 10-16 mg/mL. Crystals were grown at 18 °C using the sitting drop vapor diffusion method by mixing 1 μL Ras/Raf-RBD-CRD and 1 μL reservoir solution, with 90 μL in the reservoir. Reservoir consisted of 200 mM calcium acetate, 100 mM sodium cacodylate pH 6.5, 18% PEG 8000 (Hampton Research). Both complexes

crystallized with symmetry of the space group P321. X-ray diffraction data were collected for both complexes at the Argonne National Laboratory, Advanced Photon Source (APS) and processed with HKL2000 (Otwinowski and Minor, 1997) (details in Supplemental Information). Molecular replacement promptly placed the Ras molecule (PDB code 3K8Y) (Buhrman et al., 2010) as well as the RBD domain of Raf (taken from the Raps-GppNHp/Raf-RBD complex with PDB code 1GUA) (Nassar et al., 1996), resulting in clear electron density for both with the CRD domain clearly disordered (Supplemental Information, Figure S2).

Molecular dynamics simulations

Molecular dynamics simulations (90 ns production time) were performed for wild type Ras and RasQ61L in the absence and presence of Raf-RBD, as well as for Raf-RBD alone, at the high-performance Biowulf Linux cluster at the National Institutes of Health, Bethesda, MD (http://biowulf.nih.gov) and at the Northeastern Discovery Cluster (http://www.northeastern.edu/rc). The starting coordinates for these simulations, with the GTP analogue, GppNHp, in each coordinate set changed to GTP by replacing the β-γ-bridging nitrogen atom with oxygen, were as follows: Ras-GTP (PDB code 3K8Y), RasQ61L-GTP (PDB code 3OIU), Ras-GTP/Raf-RBD (PDB code 4G0N), RasQ61L/Raf-RBD (PDB code 4G3X) and Raf-RBD (PDB code 1RRB, average NMR structure). All crystallographic water molecules were included in the simulations of the four models solved by X-ray crystallography. The calcium and acetate ions bound in the allosteric site were retained in the coordinates for Ras-GTP, RasQ61L-GTP and Ras-GTP/Raf-RBD. The allosteric site was empty in the RasQ61L-GTP/Raf-RBD complex. DTE was deleted from the active site in the Ras/Raf-RBD structure. Residues 64 and 65, which are missing in this structure (PDB code 4G0N), were added to the model in the conformation found in Ras-GppNHp structure (PDB code 3K8Y). All simulations were performed with NAMD software using the CHARMM27 force field (Brooks et al., 2009; MacKerell et al., 1998; Phillips et al., 2005) (protocol in Supplemental Information). Dynamical network analysis was done as previously published (Sethi et al., 2009) and described further in the Supplemental Information.

Supplementary Material

Refer to Web version on PubMed Central for supplementary material.

Acknowledgments

Thanks to Paul Swartz, Michael Sawaya and Tom Terwillinger for answering questions on solving the crystal structures. Use of the Advanced Photon Source at the Argonne National Laboratory was supported by the United States Department of Energy, Office of Sciences, under Contract W31-109-Eng-38. This research was supported by grants from the NIH (R01-CA086967) and the NSF (MCB-1244203) and by the Intramural Research Program of the NIH, National Cancer Institute, Center for Cancer Research. This project has been funded in part with Federal funds from the National Cancer Institute, National Institutes of Health, under contract number HHSN261200800001E. The content of this publication does not necessarily reflect the views or policies of the Department of Health and Human Services, nor does mention of trade names, commercial products, or organizations imply endorsement by U.S. Government.

References

Baussand J, and Kleinjung J (2013). Specific Conformational States of Ras GTPase upon Effector Binding. Journal of chemical theory and computation 9, 738–749. [PubMed: 23316125]

Bondeva T, Balla A, Varnai P, and Balla T (2002). Structural determinants of Ras-Raf interaction analyzed in live cells. Molecular Biology of the Cell 13, 2323–2333. [PubMed: 12134072]

Brooks BR, Brooks CL 3rd, Mackerell AD Jr., Nilsson L, Petrella RJ, Roux B, Won Y, Archontis G, Bartels C, Boresch S, et al. (2009). CHARMM: the biomolecular simulation program. Journal of Computational Chemistry 30, 1545–1614. [PubMed: 19444816]

Buhrman G, Holzapfel G, Fetics S, and Mattos C (2010). Allosteric modulation of Ras positions Q61 for a direct role in catalysis. Proceedings of the National Academy of Sciences of the United States of America 107, 4931–4936. [PubMed: 20194776]

Buhrman G, Kumar VS, Cirit M, Haugh JM, and Mattos C (2011a). Allosteric modulation of Ras-GTP is linked to signal transduction through RAF kinase. The Journal of Biological Chemistry 286, 3323–3331. [PubMed: 21098031]

Buhrman G, O'Connor C, Zerbe B, Kearney BM, Napoleon R, Kovrigina EA, Vajda S, Kozakov D, Kovrigin EL, and Mattos C (2011b). Analysis of binding site hot spots on the surface of Ras GTPase. Journal of Molecular Biology 413, 773–789. [PubMed: 21945529]

Buhrman G, Wink G, and Mattos C (2007). Transformation efficiency of RasQ61 mutants linked to structural features of the switch regions in the presence of Raf. Structure 15, 1618–1629. [PubMed: 18073111]

Cox AD, and Der CJ (2010). Ras history: The saga continues. Small GTPases 1, 2–27. [PubMed: 21686117]

Dhomen N, and Marais R (2007). New insight into BRAF mutations in cancer. Current Opinion in Genetics & Development 17, 31–39. [PubMed: 17208430]

Drosten M, Dhawahir A, Sum EY, Urosevic J, Lechuga CG, Esteban LM, Castellano E, Guerra C, Santos E, and Barbacid M (2010). Genetic analysis of Ras signalling pathways in cell proliferation, migration and survival. The EMBO Journal 29, 1091–1104. [PubMed: 20150892]

Emerson SD, Madison VS, Palermo RE, Waugh DS, Scheffler JE, Tsao KL, Kiefer SE, Liu SP, and Fry DC (1995). Solution structure of the Ras-binding domain of c-Raf-1 and identification of its Ras interaction surface. Biochemistry 34, 6911–6918. [PubMed: 7766599]

Gohlke H, Kiel C, and Case DA (2003). Insights into protein-protein binding by binding free energy calculation and free energy decomposition for the Ras-Raf and Ras-RalGDS complexes. Journal of Molecular Biology 330, 891–913. [PubMed: 12850155]

Gohlke H, Kuhn LA, and Case DA (2004). Change in protein flexibility upon complex formation: analysis of Ras-Raf using molecular dynamics and a molecular framework approach. Proteins 56, 322–337. [PubMed: 15211515]

Gremer L, Gilsbach B, Ahmadian MR, and Wittinghofer A (2008). Fluoride complexes of oncogenic Ras mutants to study the Ras-RasGap interaction. Biological Chemistry 389, 1163–1171. [PubMed: 18713003]

Holzapfel G, Buhrman G, and Mattos C (2012). Shift in the equilibrium between on and off states of the allosteric switch in Ras-GppNHp affected by small molecules and bulk solvent composition. Biochemistry 51, 6114–6126. [PubMed: 22845804]

Huth JR, Bewley CA, Jackson BM, Hinnebusch AG, Clore GM, and Gronenborn AM (1997). Design of an expression system for detecting folded protein domains and mapping macromolecular interactions by NMR. Protein Science 6, 2359–2364. [PubMed: 9385638]

Johnson CW, and Mattos C (2013). The allostereic switch and conformational states in Ras-GTP affected by small molecules In Inhibitors of Ras Superfamily G-proteins, Tamanoi F, ed. (Elsevier), pp. 42–67.

Kearney BM, Johnson CW, Roberts DM, Swartz P, and Mattos C (2014). DRoP: A Water Analysis Program Identifies Ras-GTP-Specific Pathway of Communication between Membrane-Interacting Regions and the Active Site. Journal of Molecular Biology 426, 611–629. [PubMed: 24189050]

MacKerell AD, Bashford D, Bellott M, Dunbrack RL, Evanseck JD, Field MJ, Fischer S, Gao J, Guo H, Ha S, et al. (1998). All-atom empirical potential for molecular modeling and dynamics studies of proteins. J Phys Chem B 102, 3586–3616. [PubMed: 24889800]

Nassar N, Horn G, Herrmann C, Block C, Janknecht R, and Wittinghofer A (1996). Ras/Rap effector specificity determined by charge reversal. Nature structural biology 3, 723–729. [PubMed: 8756332]

Nussinov R, Tsai CJ, and Mattos C (2013). 'Pathway drug cocktail': targeting Ras signaling based on structural pathways. Trends in Molecular Medicine 19, 695–704. [PubMed: 23953481]

O'Connor C, and Kovrigin EL (2012). Characterization of the second ion-binding site in the G domain of H-Ras. Biochemistry 51, 9638–9646. [PubMed: 23148511]

Otwinowski Z, and Minor W (1997). Processing of X-ray diffraction data collected in oscillation mode. Method Enzymol 276, 307–326.

Phillips JC, Braun R, Wang W, Gumbart J, Tajkhorshid E, Villa E, Chipot C, Skeel RD, Kale L, and Schulten K (2005). Scalable molecular dynamics with NAMD. Journal of Computational Chemistry 26, 1781–1802. [PubMed: 16222654]

Prior IA, Lewis PD, and Mattos C (2012). A comprehensive survey of Ras mutations in cancer. Cancer Research 72, 2457–2467. [PubMed: 22589270]

Roskoski R Jr. (2010). RAF protein-serine/threonine kinases: structure and regulation. Biochemical and Biophysical Research Communications 399, 313–317. [PubMed: 20674547]

Sethi A, Eargle J, Black AA, and Luthey-Schulten Z (2009). Dynamical networks in tRNA:protein complexes. Proceedings of the National Academy of Sciences of the United States of America 106, 6620–6625. [PubMed: 19351898]

Spoerner M, Hozsa C, Poetzl JA, Reiss K, Ganser P, Geyer M, and Kalbitzer HR (2010). Conformational states of human rat sarcoma (Ras) protein complexed with its natural ligand GTP and their role for effector interaction and GTP hydrolysis. The Journal of Biological Chemistry 285, 39768–39778. [PubMed: 20937837]

Terada T, Ito Y, Shirouzu M, Tateno M, Hashimoto K, Kigawa T, Ebisuzaki T, Takio K, Shibata T, Yokoyama S, et al. (1999). Nuclear magnetic resonance and molecular dynamics studies on the interactions of the Ras-binding domain of Raf-1 with wild-type and mutant Ras proteins. Journal of Molecular Biology 286, 219–232. [PubMed: 9931261]

Thapar R, Williams JG, and Campbell SL (2004). NMR characterization of full-length farnesylated and non-farnesylated H-Ras and its implications for Raf activation. Journal of Molecular Biology 343, 1391–1408. [PubMed: 15491620]

Highlights

- Crystal structures of HRas and HRasQ61L have been solved in complex with Raf-RBD.
- The Q61L mutation has global effects on Ras and Raf-RBD in the complex.
- The Q61L mutation changes flexibility at interface linking to Raf-RBD loop L4.
- Ras mutants can contribute to oncogenesis beyond local effects on the active site.

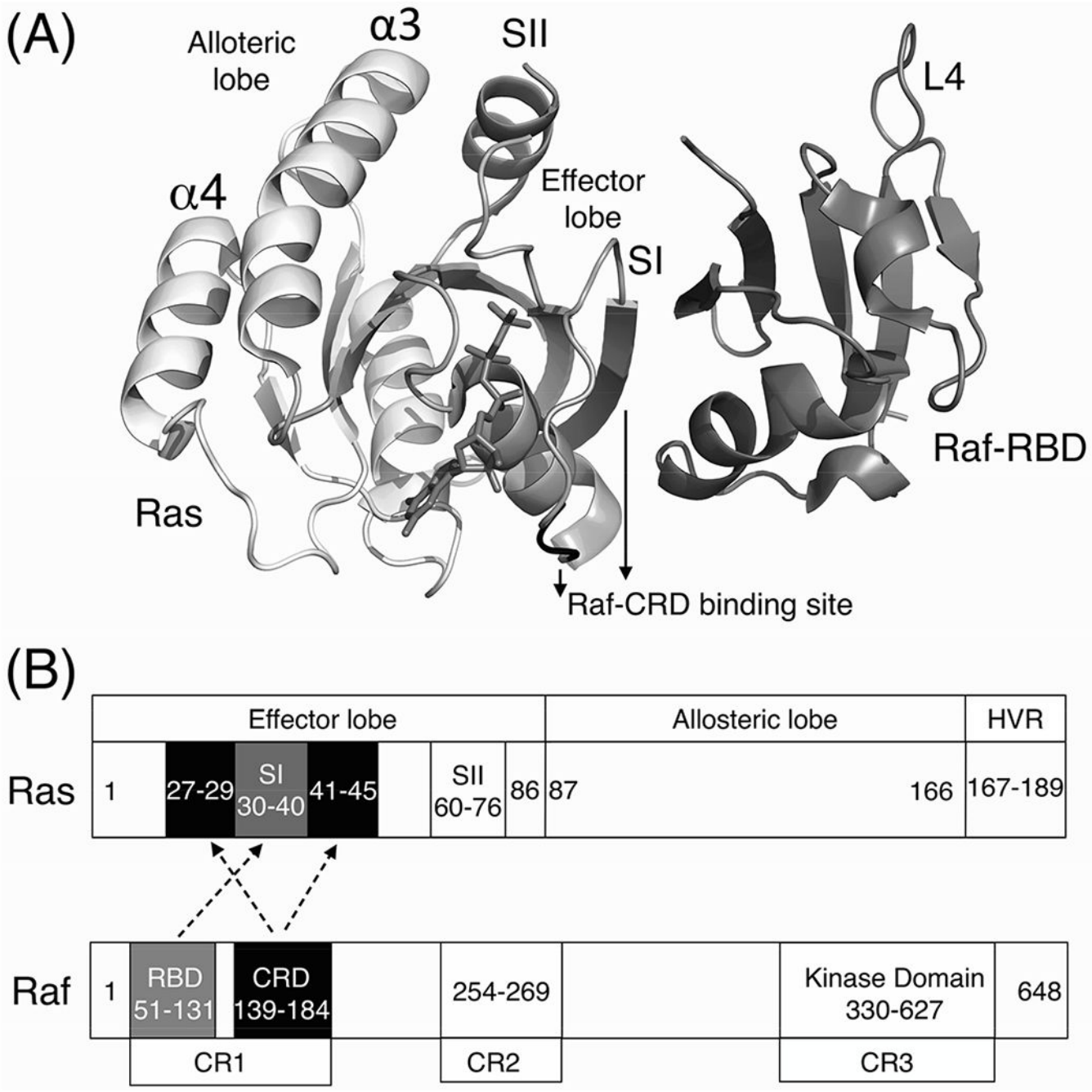

Figure 1.

The Ras and Raf proteins. (A) Ribbon diagram of the Ras/Raf-RBD complex. The Ras effector lobe is in light gray and the allosteric lobe is in white. Regions of Ras known to interact with Raf-CRD are in black and the Raf-RBD domain is in dark gray. (B) Schematic of the Ras and Raf sequences. Location of the two lobes of Ras and the various domains of Raf are shown. Dashed lines identify regions known to interact in the complex. Schematics for Ras and Raf are not to scale.

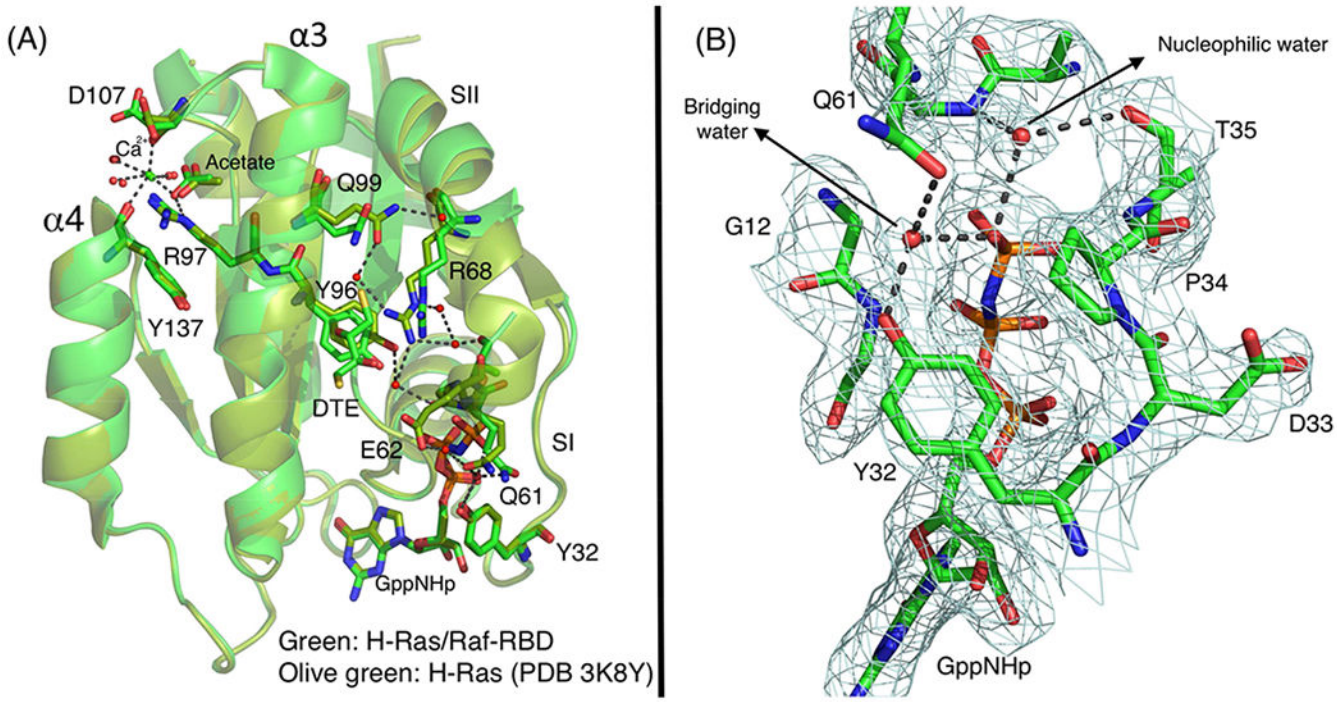

Figure 2.

The wild type Ras structure in the complex with Raf-RBD. (A) Superposition of Ras in the Ras/Raf-RBD complex and our structure of Ras solved in the R32 crystal form with PDB code 3K8Y. Residues involved in the allosteric switch to promote the R state are shown in stick. Calcium and acetate are bound in the allosteric site. In the Ras model with PDB code 3K8Y black dashed lines indicate the hydrogen-bonding network from the allosteric site to the active site, with the water molecules shown as red spheres. (B) Active site of Ras in the Ras/Raf-RBD complex with electron density contoured at the 1.0σ level.

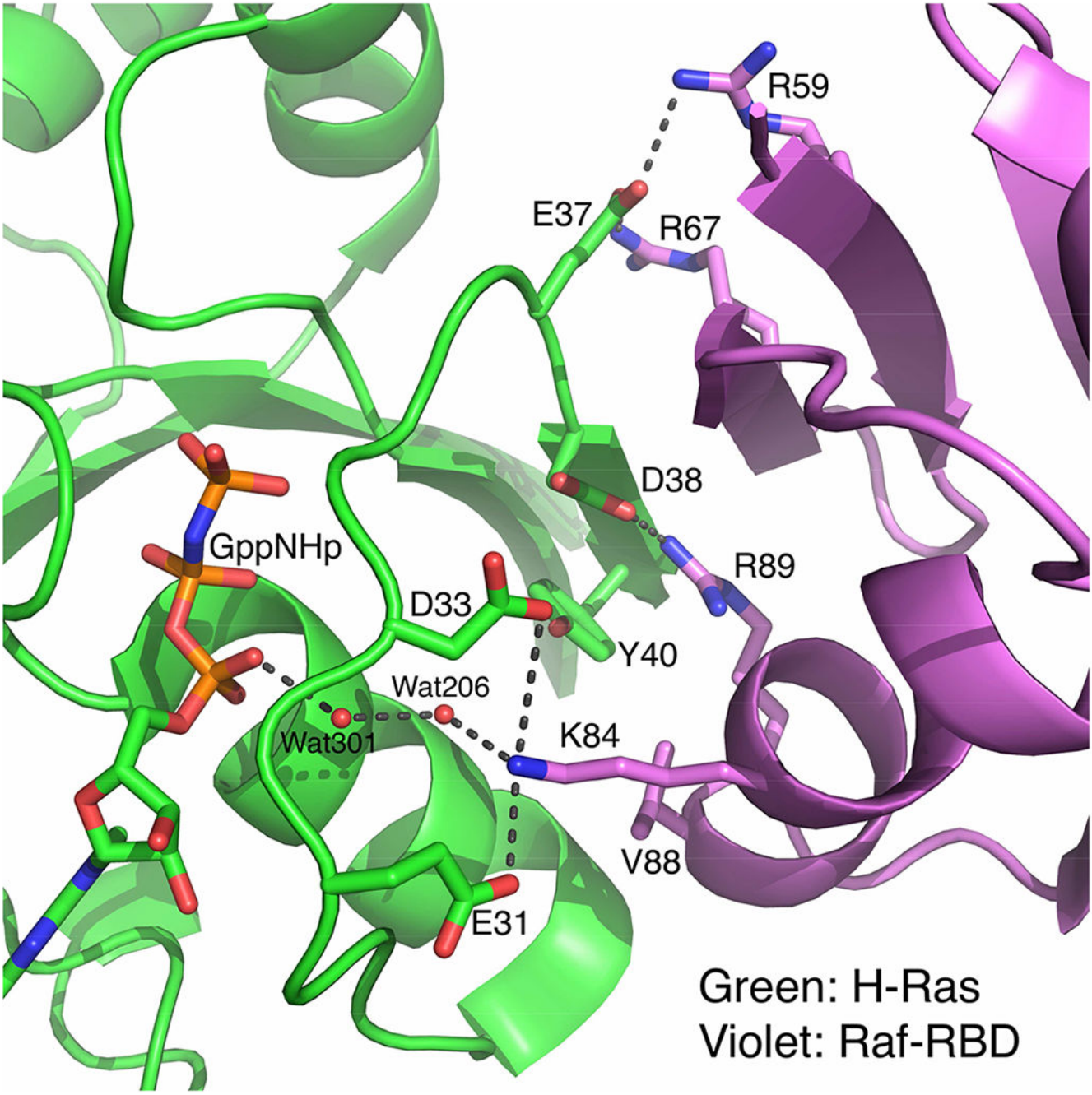

Figure 3.

The wild type Ras/Raf-RBD interface. Residues involved in salt bridges, H-bonding and van der Waals interactions across the interface are shown in stick. Water molecules are shown in red spheres and H-bonding interactions are in black dashed lines.

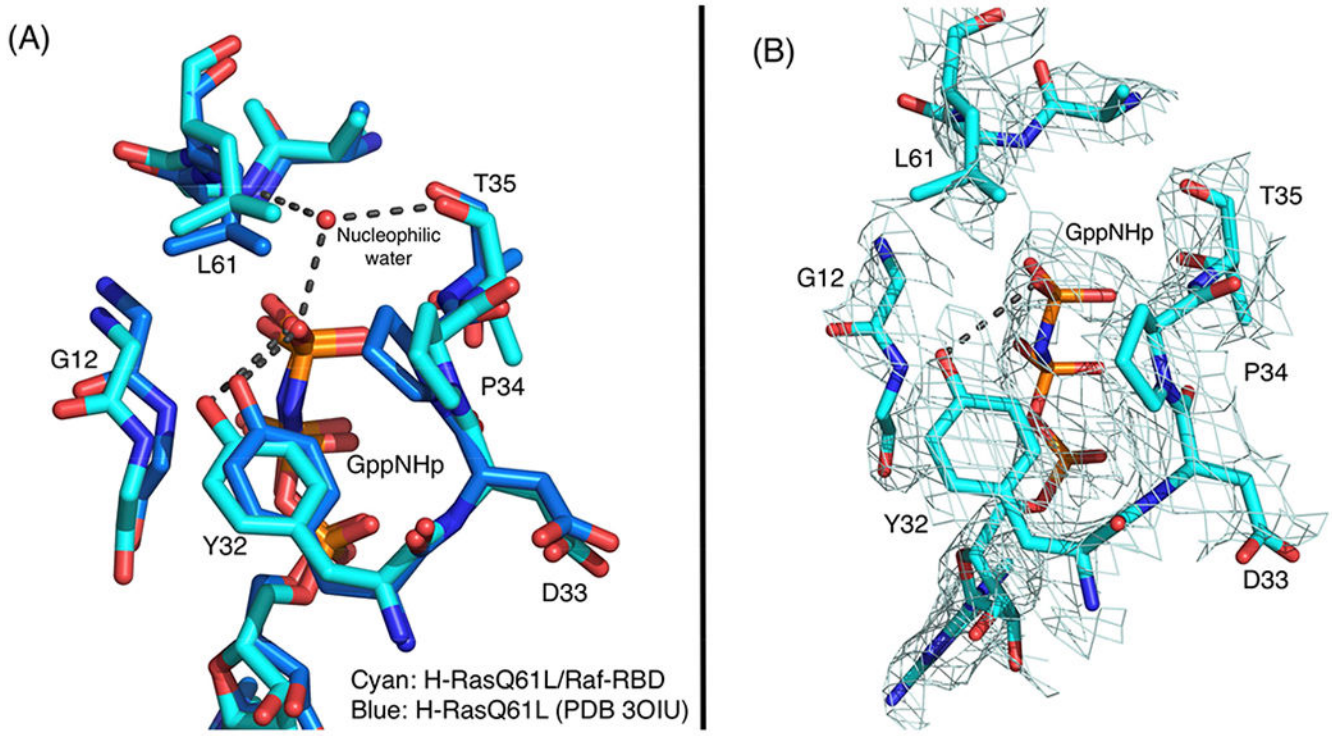

Figure 4.

The RasQ61L structure in the complex with Raf-RBD. (A) Active site in the mutant complex superimposed on the structure of the RasQ61L mutant solved from crystals with R32 symmetry with PDB code 3OIU. The water molecule shown in red sphere is from the structure with PDB code 3OIU. (B) Active site of RasQ61L in the RasQ61L/Raf-RBD complex. The electron density is contoured at the 1.0σ level.

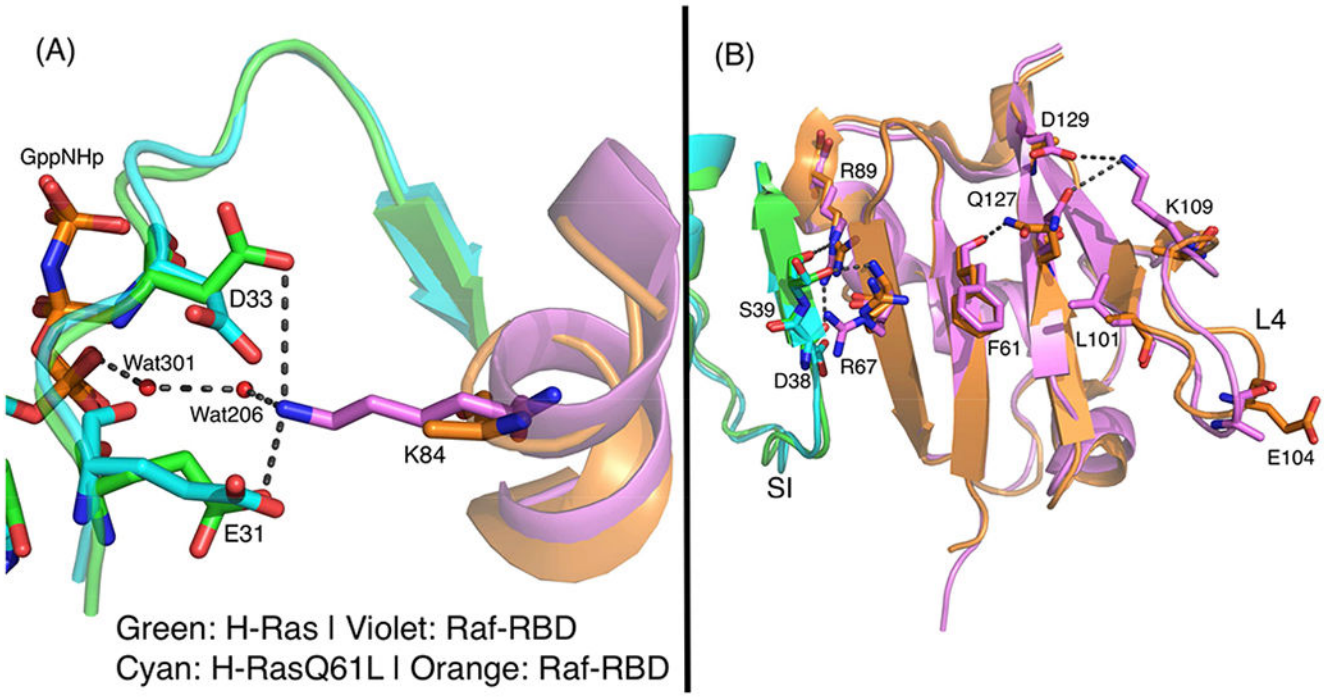

Figure 5.

Changes in Raf-RBD due to the Q61L mutation in Ras. (A) K84 at the Ras/Raf-RBD interface. In the mutant complex there is no electron density for K84 beyond the Cβ atom and the side chain has been truncated accordingly. The water molecules shown in red spheres and the hydrogen bonds indicated by black dashed lines belong the wild type Ras/Raf-RBD complex. (B) Changes that propagate from the interface to Raf-RBD loop L4 containing E104. There is no electron density beyond the Cβ atoms for residues L101, K109 and D129 in the mutant complex and these side chains have been truncated accordingly.

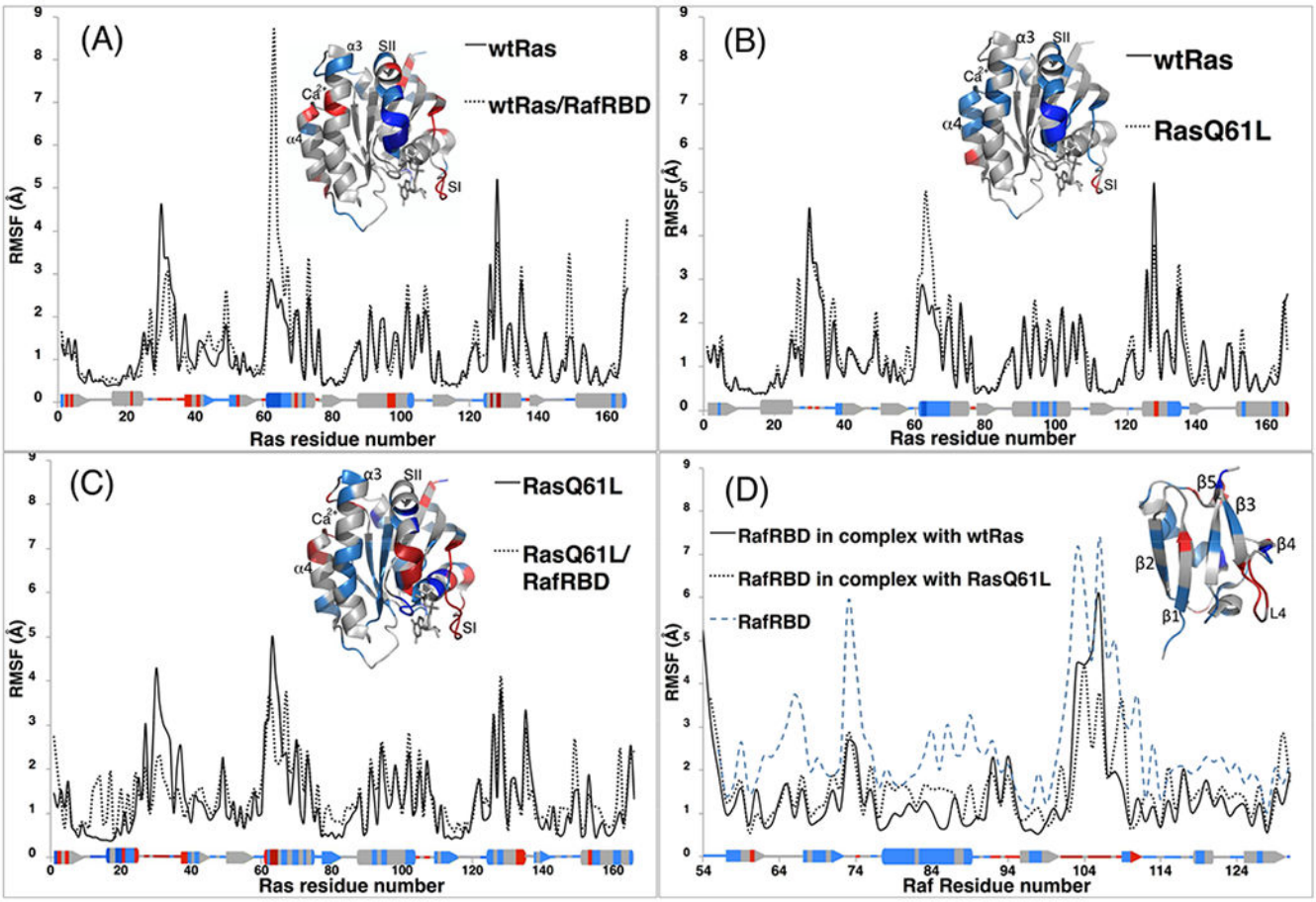

Figure 6.

Average Cα root-mean-square-fluctuations (RMSFs) for Ras and Raf-RBD. Protein secondary structures are shown along the x-axis of the plots. Protein structures in the inserts are shown in gray with increases in fluctuations shown in blue and decreases shown in red (>0.25 Å, with colors darkening as the change increases). Corresponding colors are shown in the x-axis on the RMSF plots. The two switches are labeled SI and SII. (A) Uncomplexed wild type Ras (wtRas) and wtRas bound to Raf-RBD. The Ras structure shows the effect of binding Raf-RBD. (B) Uncomplexed wtRas and uncomplexed RasQ61L. Ras structure shows the effect of the Q61L mutation on uncomplexed Ras. (C) Uncomplexed RasQ61L and RasQ61L bound to Raf-RBD. The Ras structure shows the effect of binding Raf-RBD to the RasQ61L mutant. (D) Uncomplexed Raf-RBD, Raf-RBD bound to wtRas and Raf-RBD bound to RasQ61L. Raf-RBD structure shows the effect of RasQ61L relative to wtRas on the complexed Raf-RBD protein.

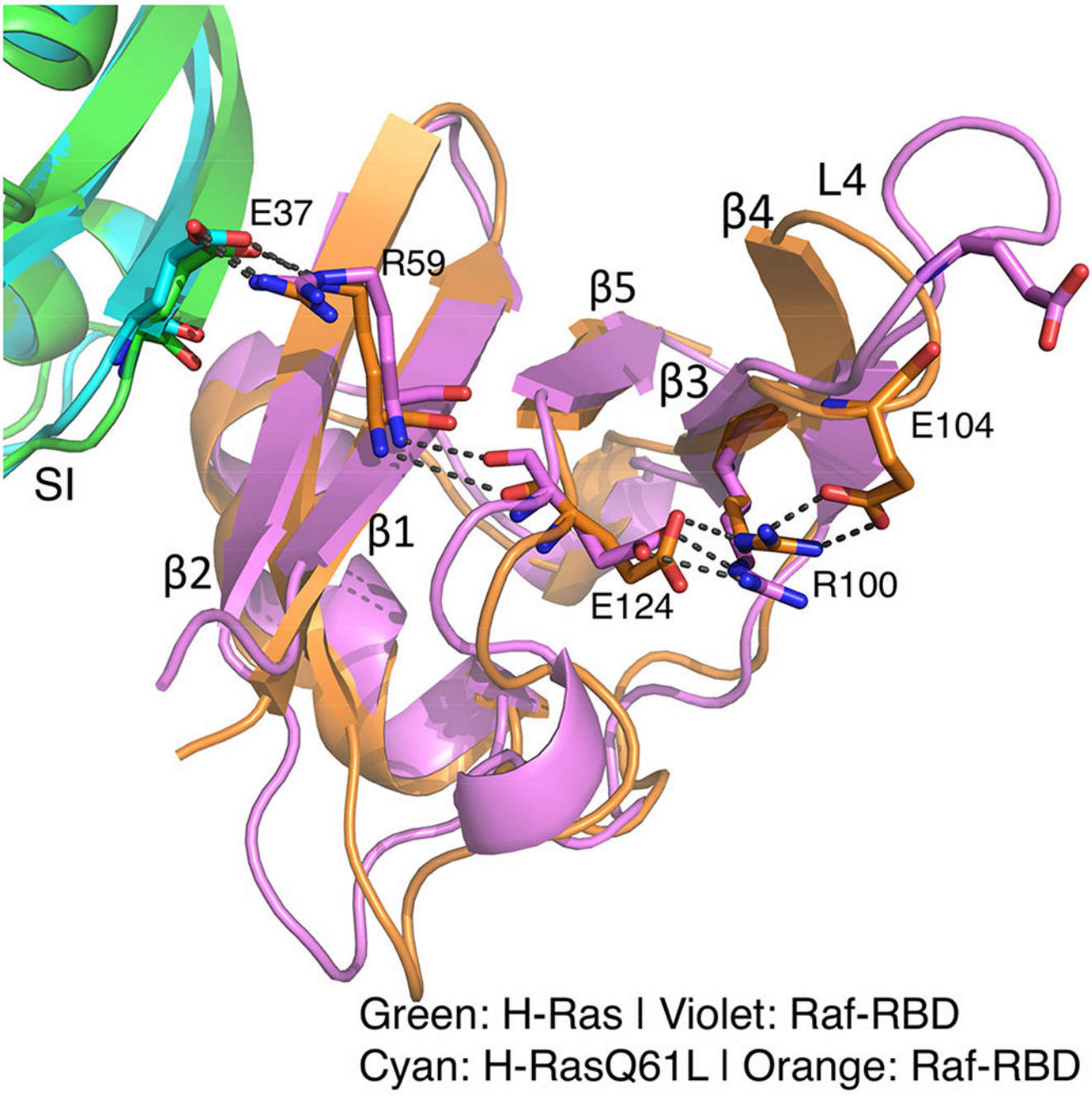

Figure 7.

Average MD simulation structures for Ras/Raf-RBD and RasQ61L/Raf-RBD. The H-bonding/salt bridge network from RasQ61L residue E37 to Raf-RBD E104 in L4 is shown for the mutant complex. E104 does not interact with this network in the wild type complex. The color-coding is as in Figure 5.

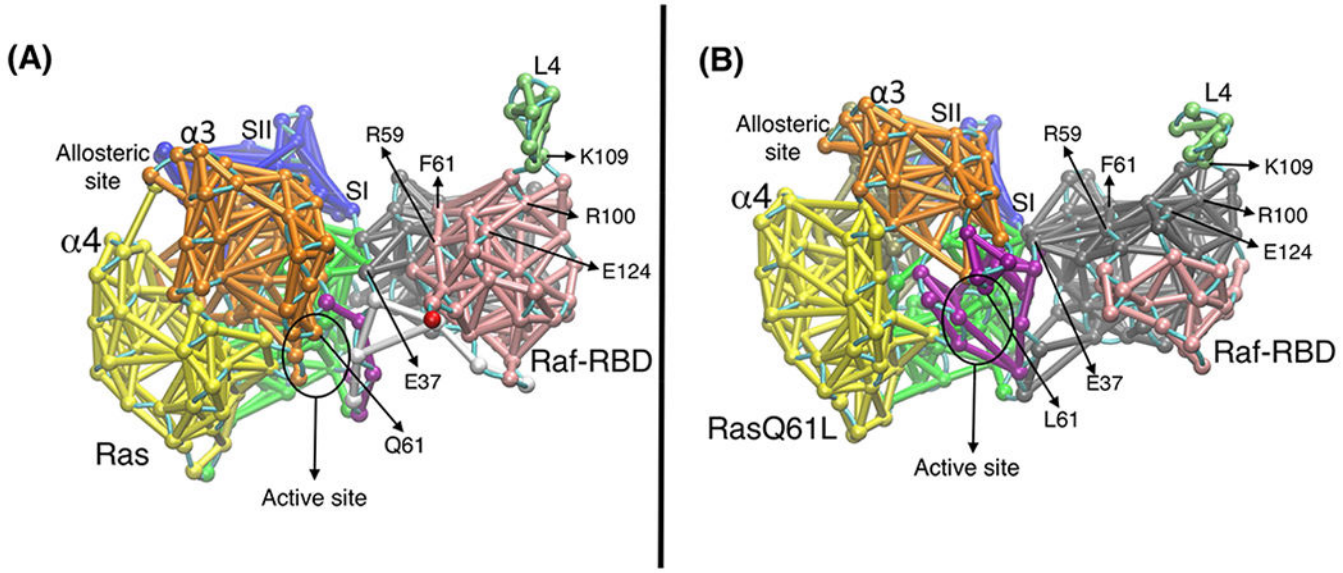

Figure 8.

Community networks formed in the Ras/Raf-RBD complexes based on MD simulations. Each community has its own color, superimposed on the respective average MD simulation structure. (A) Wild type Ras/Raf-RBD. The allosteric site and active site residue Q61 are in the network community shown in orange. Two communities, gray and pink, separate the interface from L4. (B) RasQ61L/Raf-RBD. The allosteric site and Q61 are in two separate communities, orange and magenta, respectively. The interface is linked to L4 through the network community shown in gray.

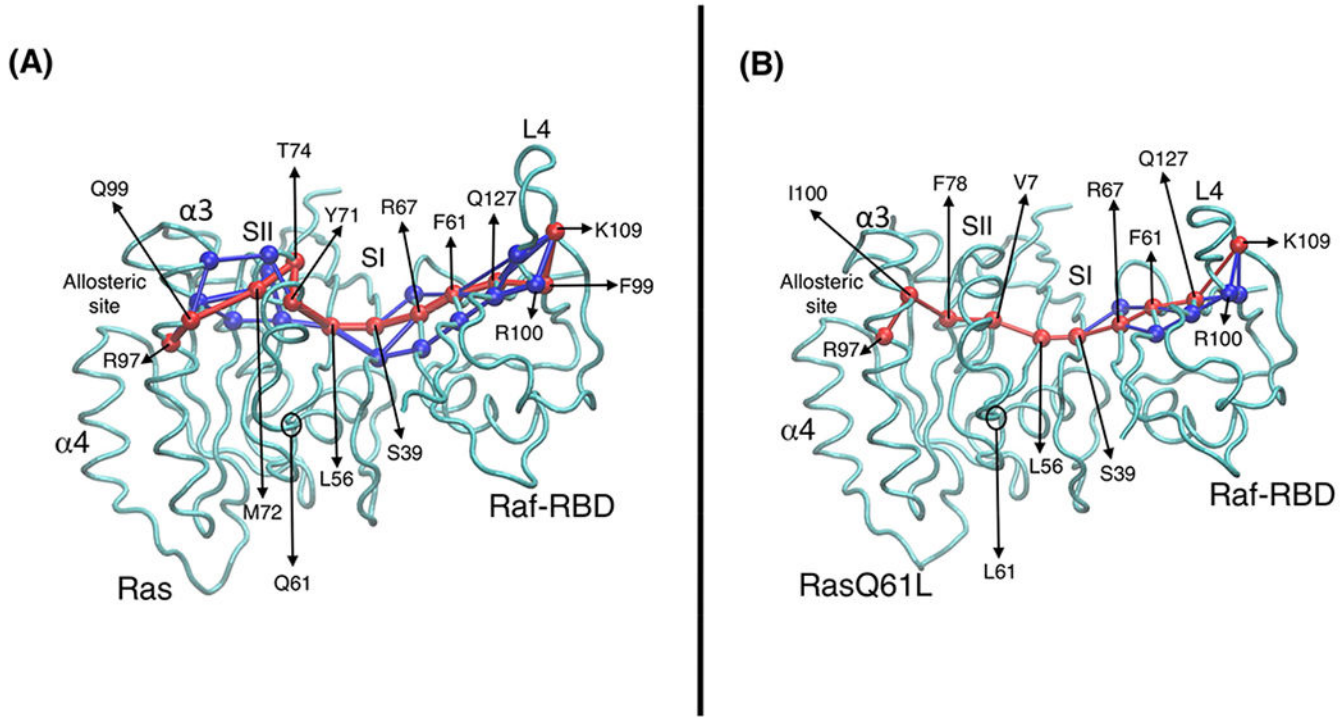

Figure 9.

Optimal and suboptimal paths connecting R97 in the Ras allosteric site to K109 at the end of Raf-RBD loop L4. (A) The optimal path (red) and several suboptimal paths (blue) found for the wild type Ras/Raf-RBD complex. There are 39 suboptimal paths in this complex. (B) The optimal path (red) and suboptimal paths (blue) found for the RasQ61L/Raf-RBD complex. Only 6 suboptimal paths are found in in the mutant complex. The backbone trace of the Ras and Raf-RBD corresponding to the average MD simulation structures of the complexes are shown in cyan. Spheres indicate residue nodes in the paths. The thickness of each edge is proportional to the number of suboptimal paths that cross it during the calculation. Note the thin edges in the mutant complex. Residue identities for the nodes in the optimal paths for both complexes are given, as well as for other residues and structural features discussed in the text.

Table 1.

Data Collection and Refinement Statistics

Data Collection	**WT Ras/Raf-RBD**	**RasQ61L/Raf-RBD**
PDB entry	4G0N	4G3X
Space group	P321	P321
Cell Dimensions		
a, *b*, *c* (Å)	90.44, 90.44, 92.70	91.40, 91.40, 93.11
α, β, γ	90, 90, 120	90, 90, 120
Resolution (Å)	50–2.45 (2.48–2.45)	50–3.25 (3.31–3.25)
R_{sym}	0.146 (0.649)	0.179 (0.477)
I/σ	25.0 (2.0)	26.0 (1.5)
Completeness (%)	97.6 (74.1)	87.4 (55.6)
Redundancy	8.9 (3.5)	4.6 (3.4)
Wilson *B* (Å^2)	36.8	46.2
Refinement		
Resolution (Å)	50–2.45	50–3.28
Reflections (total)	16,133	6,462
R_{work}/R_{free}	0.181/0.229	0.251/0.271
Average *B* factor (Å^2)	59.0	63.0
No. of atoms		
Protein	1,875	1,860
Water	82	17
Total	2,004	1,918
No. of molecules		
Organic	3	1
Metals	3	1
Root-mean-square deviation		
Bond length (Å)	0.007	0.009
Bond angle (°)	0.680	0.597
Ramachandran (%)		
Preferred region	97.0	81.0

$R_{sym} = \Sigma|I_i - \langle I \rangle| / \Sigma I \cdot R_{work} = \Sigma||F_O| - |F_C|| / \Sigma|F_O|$, calculated by using 90% of the reflections against which the model was refined. $R_{free} = \Sigma||F_O| - |F_C|| / \Sigma|F_O|$, calculated by using a test set consisting of 10% of the total reflections, randomly selected from the original data set. Parentheses include information for the highest-resolution shell.